Enhancement of the Synthetic Storm Technique for the Prediction of Rain Attenuation Time Series at EHF

Lorenzo Luini, *Senior Member*, *IEEE*, Alberto Panzeri,
Carlo Riva, *Senior Member*, *IEEE*

***Abstract* — A physically-based rain attenuation prediction model for Earth-space links, namely the Enhanced Synthetic Storm Technique (E-SST), is presented. Differently from the original SST, the E-SST receives as input detailed information on the rain height and on the storm velocity, and it discriminates between stratiform and convective rain events having a different impact on the link. The rain attenuation prediction accuracy of E-SST, both as applied directly and as embedded into a more accurate frequency scaling technique, is evaluated against a full year of propagation data collected by the NASA equipment installed at Politecnico di Milano in the frame of the Alphasat Aldo Paraboni propagation experiment. To this aim, a novel methodology to isolate the contribution of rain attenuation from the received beacon power is devised and presented. Results indicate that E-SST represents an accurate and reliable tool for the prediction of rain attenuation at EHF, both on a statistical basis (direct application) and on an event basis (frequency scaling).**

***Index Terms* — Rain attenuation, Synthetic Storm Technique, frequency scaling, satellite communications.**

I. INTRODUCTION

Tropospheric effects severely impair the propagation of centimetric and millimetric electromagnetic waves. Clouds, gases (namely water vapor and oxygen) and hydrometeors are the main atmospheric components interacting with EM waves in the 1-1000 GHz range [1]. The impact of precipitation becomes relevant and predominant above 10 GHz, as the wavelength is comparable with the dimension of rain drops, which cause absorption and scattering of the electromagnetic energy [2].

As a consequence, the accurate prediction of the attenuation induced by rain remains an essential task in order to properly design reliable Earth-space links in satellite communication (SatCom) systems, as well as in Earth Observation (EO) and in Space Exploration (SE) missions. In fact, rain attenuation prediction is becoming more and more critical in the light of the increase in the carrier frequencies that all the systems mentioned above are gradually facing (shift from the Ka to the Q/V bands for SatCom systems [3], and from the X to the Ka band for EO and SE missions [4]), which calls for the need of even more accurate and reliable prediction models. On the one hand, the optimum prediction method should rely on a sound physical basis to guarantee a high level of reliability, especially when applied to achieve predictions at frequencies for which no experimental measurements are yet available (e.g. W band [5]); on the other hand, such model should not just provide statistical results, but also enable to predict time series of the rain attenuation A for the design and operation of the necessary fade mitigation techniques, such as site diversity [6], whose effectiveness is tightly linked to the dynamics of A (e.g. fade slope and fade duration).

Some physically-based rain attenuation models exist in the literature, but they can be typically applied only on a statistical basis (e.g. [7], [8] and [9] to cite a few); on the other hand, time series synthesizers, such as [10], generate time series of A, but they are of stochastic nature, i.e. with a limited physical soundness, and, moreover, they require as input the statistics of A.

Among the plethora of the available rain attenuation prediction models, the Synthetic Storm Technique (SST), firstly presented in [11] and extended in [12] to Earth-space links, emerges as a unique methodology combining the advantages of a sound physical-mathematical framework, of the applicability on a statistical basis and on an event basis, and of the need of limited inputs (time series of the rain rate). Notwithstanding this, the SST presents a limitation associated to how the effect of the melting layer is modeled, which is addressed in this contribution with the aim of improving the model's prediction accuracy. This goal is achieved also by providing more refined data as input to SST (rain height and storm translation velocity). The proposed methodology, henceforth referred to as Enhanced SST (E-SST), is tested against the propagation data collected by NASA equipment installed at Politecnico di Milano during the whole of 2017 in the frame of the Alphasat Aldo Paraboni propagation experiment [13]. To this aim, a new methodology to isolate the contribution of rain attenuation from the received beacon

Manuscript received XXXX.

Lorenzo Luini and Carlo Riva are with the Dipartimento di Elettronica, Informazione e Bioingegneria, Politecnico di Milano, Piazza Leonardo da Vinci, 32, 20133, Milano, Italy, and with the Istituto di Elettronica e di Ingegneria dell'Informazione e delle Telecomunicazioni (IEIIT), Consiglio Nazionale delle Ricerche, Via Ponzio 34/5, Milano 20133, Italy (e-mail: lorenzo.luini@polimi.it).

Alberto Panzeri is with the Dipartimento di Elettronica, Informazione e Bioingegneria, Politecnico di Milano, Piazza Leonardo da Vinci, 32, 20133, Milano, Italy.

power is devised by relying on the combination of multiple ancillary instruments and data.

The remainder of this paper is structured as follows. Section II presents the experimental setup and describes the methodology to derive rain attenuation from the received beacon signals (two frequency bands). Section III introduces E-SST by highlighting its key features adopted to enhance the performance of SST. Section IV deals with the presentation, discussion and evaluation of the results obtained from the use of E-SST, both when applied directly and when embedded into an even more accurate frequency scaling approach. Finally, Section V draws some conclusions.

II. Experimental Setup and Data Processing

A. The Experimental Equipment

The data used in this contribution are collected in the frame of the Alphasat Aldo Paraboni propagation experiment [13], which is supported by the Italian Space Agency (ASI), and executed by the European Space Agency (ESA), to achieve a better understanding of the atmospheric propagation channel at frequencies in the Ka and Q bands. The space segment of the experiment includes the Alphasat satellite, a geosynchronous satellite owned by Inmarsat (25° East orbital position), which also embarks the Aldo Paraboni payload, featuring two continuous-wave beacons at 19.701 GHz and 39.402 GHz.

A receiving station is installed on the rooftop of a building in the main campus of Politecnico di Milano in Milan, Italy (latitude 45.48° N, longitude 9.23° E, altitude 137 m a.m.s.l.). As shown in Fig. 1, the experimental equipment, developed and owned by NASA Glenn Research Center (GRC), includes two receivers recording the beacon power at 8 samples/second. The diameter of the receiving antennas is 1.2 m (Ka band) and 0.6 m (Q band), respectively, and both receivers are equipped with a step motors to track the Alphasat satellite, whose orbital plane has a variable inclination angle, slowly drifting up to 3° (the average link elevation angle in Milan is 35.6°).

In addition, collocated with the beacon receivers are:

- A weather station, measuring pressure P, temperature T and relative humidity RH at ground level.
- A tipping bucket to measure the precipitation rate R.
- A Thies Clima disdrometer operating by means of an infrared laser diode, which generates a 785 nm beam over an area of 4560 mm^2. The observed falling particles (rain, snow flakes, hail, …) are classified into spectra of 22 diameter bins from 0.125 mm to 8 mm and 20 velocity bins from 0 to 10 m/s with non-uniform bin widths.
- A multi-channel microwave radiometer (23.84, 31.4, 72.5 and 82.5 GHz), MWR, pointed along the path to the Alphasat satellite to derive the integrated liquid water content and the integrated water vapor content, from which the tropospheric attenuation, in nonrainy conditions, can be in turn calculated.

The experimental dataset is completed by vertical profiles of the atmosphere obtained from RAOBS (radiosonde observations) data (Milano Linate Airport, 5 km from the experimental site, launches performed twice a day) and from ECMWF (European Centre for Medium-range Weather Forecast) NWP products, specifically extracted from the ERA5 database: the main advantages of ERA5 are its accuracy (it is the most recent re-analysis carried out by the ECMWF), and its rather fine resolution (0.28125°×0.28125° horizontal resolution, 137 vertical levels, data available every hour).

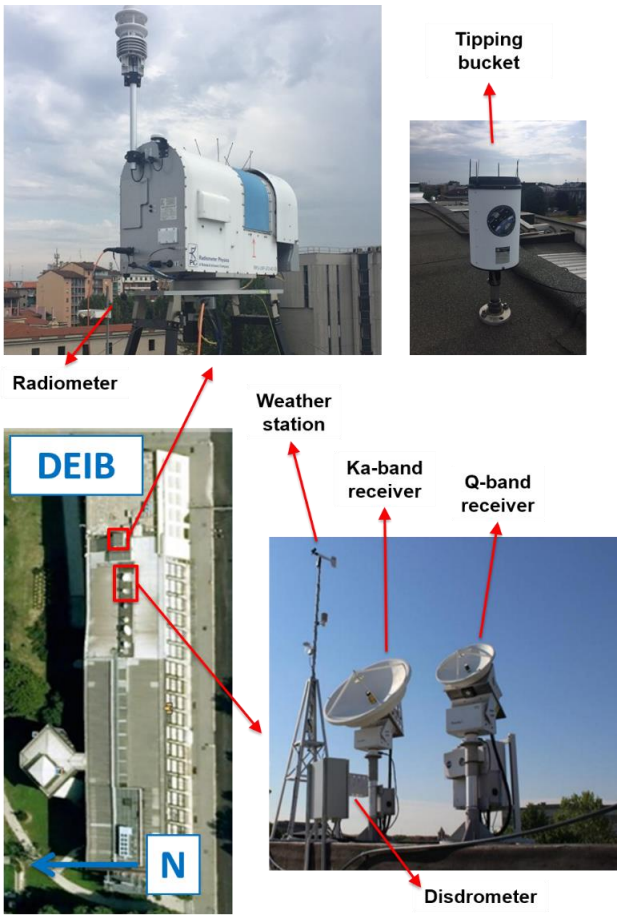

Fig. 1. NASA experimental equipment installed on the rooftop of the Dipartimento di Elettronica, Informazione e Bioingegneria (DEIB) of Politecnico di Milano.

B. Processing of Disdrometer Data

One of the paramount objectives of electromagnetic wave propagation experiments is to measure the attenuation due to rain, which can be extracted from the received beacon signal, once rain events are identified: to this aim, disdrometer data are key. As a first step, such data are combined to calculate the Drop Size Distribution (DSD) $N(D)$, which indicates the number of rain drops with given diameter D per m^3 [14]:

$$N(D_i) = \frac{10^6 n_i}{S\, v(D_i)\, T\, \Delta D_i} \quad (\text{mm}^{-1}\,\text{m}^{-3}) \tag{1}$$

In (1), n_i is the number of raindrops whose diameter falls in the i-th class (with mean diameter D_i), ΔD_i (mm) represents the width of each drop-size class, S (mm^2) is the disdrometer sampling area, T (seconds) is the instrument integration time, $v(D_i)$ (m/s) is the rain drop falling velocity.

The rain rate R (mm/h) is then derived from the DSD as:

$$R = 600 \cdot 10^{-6} \pi \sum_{i=1}^{N} N(D_i) D_i^3 v(D_i) \Delta D_i \quad (2)$$

C. Vertical Atmospheric Profiles

The vertical atmospheric profiles retrieved from the ERA5 database are processed to extract the 0 °C isotherm height (h_0) and the wind speed associated to the 700-mbar isobar height (v): in fact, the former is typically considered as a good estimate of the rain height (especially during stratiform events) [7], while the latter has been proven to be well correlated to the precipitation translation velocity [15]. Both h_0 and v represent key input information for the prediction model presented in this contribution.

D. Processing of Beacon Data to Extract Rain Attenuation

Isolating the contribution of rain from the total attenuation induced by the atmosphere is not a trivial task.

The typical well-established approach to derive rain attenuation from the received beacon power P is to first low-pass filter P to remove scintillations with typical cut-off frequency of 0.03 Hz. Afterwards, rain events are identified, usually both by taking advantage of the local rain sensors (if present) and by inspecting the trend of P; finally, the rain attenuation A_R is calculated by subtracting from P the power level that is the linear interpolation of P just before the beginning and the end of the each event [16].

Though simple, this approach does not actually isolates A_R, but rather the so called "excess attenuation", i.e. a combination of the attenuation due to rain and clouds; as a matter of fact, the cloud attenuation A_C is expected to increase during rain events, and this cannot be taken into account by the procedure mentioned above, which, in fact, limits A_C to the values observed before and after the rain event, due to the interpolation procedure mentioned above. As the attenuation due to clouds becomes more and more relevant with frequency increasing from the Ku/Ka bands to Q/V bands, an alternative more accurate approach to separate rain attenuation and cloud attenuation is proposed hereinafter.

As a first step, the total atmospheric attenuation A is derived from the received beacon power P by taking advantage of the collocated MWR, which allows estimating, with very high accuracy, the total tropospheric attenuation in non-rainy conditions A^{MWR}, starting from brightness temperature data T_B collected at (at least) two channels. The full procedure to derive A from P, which is well established and has been employed in several propagation experiments (e.g. [17]) when radiometric data are available, is duly detailed in [18].

The first step to derive rain attenuation is to remove scintillations from the total attenuation by low-pass filtering A, as already mentioned above. The next step is to subtract from A the contribution of atmospheric gases, i.e. oxygen and water vapor. To this aim, radiometric measurements can again be used. More specifically, the gaseous attenuation A_G^{MWR} is calculated by removing the cloud attenuation A_C^{MWR} from the MWR-derived total tropospheric attenuation A^{MWR}:

$$A_G^{MWR} = A^{MWR} - A_C^{MWR} = A^{MWR} - a_L L \quad (3)$$

Equation (3) indicates that the cloud attenuation is calculated by using the liquid water mass absorption coefficient $a_L(f)$ and the liquid water content integrated along the path L; the former is extracted from Recommendation ITU-R P.840-7 (equation (14) in [19]), which provides a_L(19.7 GHz) = 0.391 dB/mm and a_L(39.4 GHz) = 1.338 dB/mm, while the latter is retrieved again from the radiometric measurements using the well-established simple linear inversion model reported in [20]. It is worth stressing that, as radiometric retrievals of L are reliable only in rain-free conditions [20], during rain events, the value of A_G^{MWR} is interpolated between the beginning and the end of the event: this step is not expected to introduce a significant error because, differently from the attenuation due to clouds, A_G^{MWR} is likely to remain quite stable during rain events.

Taking advantage of A_G^{MWR}, the attenuation due to rain plus clouds A_{RC} is calculated as:

$$A_{RC} = A - A_G^{MWR} \quad (4)$$

As a final step, the cloud attenuation A_C and the rain attenuation A_R are obtained as:

$$A_C = \begin{cases} R_{RC} A_{RC} & A_{RC} \le A_{RC}^{\max} \\ A_C^{\max} & A_{RC} > A_{RC}^{\max} \end{cases} \quad (5)$$

$$A_R = A_{RC} - A_C \quad (6)$$

where:

$$R_{RC} = a \exp(-b A_{RC}) + (1-a) \exp(-c A_{RC}) \quad (7)$$

Fig. 2 shows the trend of R_{RC} for both frequencies, while Table I lists the coefficients a, b, c, and the values of $A_C^{\max}$ and $A_{RC}^{\max}$ in (5).

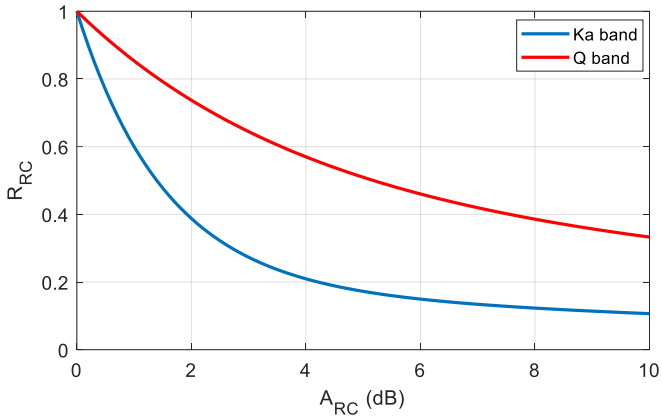

Fig. 2. Trend of R_{RC} as a function of A_{RC} for both frequencies.

TABLE I. COEFFICIENTS IN (7) AND VALUES IN (5).

	a	b	c	$A_C^{\max}$	$A_{RC}^{\max}$
Ka band	0.8089	0.6552	0.05958	1.1 dB	11 dB
Q band	0.5689	0.2589	0.03963	3.85 dB	16.9 dB

As shown in Fig. 2, R_{RC} has a monotonic decreasing trend: in fact, at the very start of the rain event, i.e. when the link is about to enter into a rain cell, the attenuation will reasonably be induced only by clouds (R_{RC} = 1 and A_R = 0); as the rain event translates more on the link, R_{RC} is expected to decrease (i.e. A_R to increase) quickly, as most of the attenuation will be due to rain; nevertheless, as A_{RC} increases, A_C will grow as well, but up to a its maximum value $A_C^{\max}$, as shown in (5). $A_C^{\max}$ was set as the A_C value exceeded for 0.01% of the yearly time, in turn obtained from the complementary cumulative distribution function (CCDF) of A_C: as an example, Fig. 3 reports the CCDF for the Q band; which was calculated from 20 years of the RAOBS mentioned in Section II.A. Specifically, as performed in [20], vertical profiles of *P-RH-T* obtained from RAOBS were used first to derive the liquid water content by means of the TKK cloud detection algorithm [21], and, afterwards, to calculate the cloud attenuation through the Liebe MPM93 mass absorption model [22]. $A_C^{\max}$ represents a reliable indication of the top values of A_C experienced in the site: higher values are achieved only for roughly 1 hour/year (exceedance probability of 0.01%), and their estimation is increasingly less accurate.

After setting $A_C^{\max}$ (1.1 dB and 3.85 dB, for the Ka band and Q band, respectively, as shown in Table I), the coefficients *a*, *b* and *c* in (7) were derived by optimizing the agreement between the RAOBS-derived CCDF of A_C and the one obtained from (5) using the full year of beacon-derived attenuation data *A*. The optimization procedure also involved the determination of $A_{RC}^{\max}$, which, combining (5) and (7), is calculated as the A_{RC} values obtained when A_C reaches $A_C^{\max}$.

Fig. 3 compares the CCDFs of A_C (Q band, RAOBS-derived versus beacon-derived), while Fig. 4 shows an example of the separate contributions to total attenuation (gases, clouds, and rain), obtained using the procedure outlined above (Q band, 4th of February 2017).

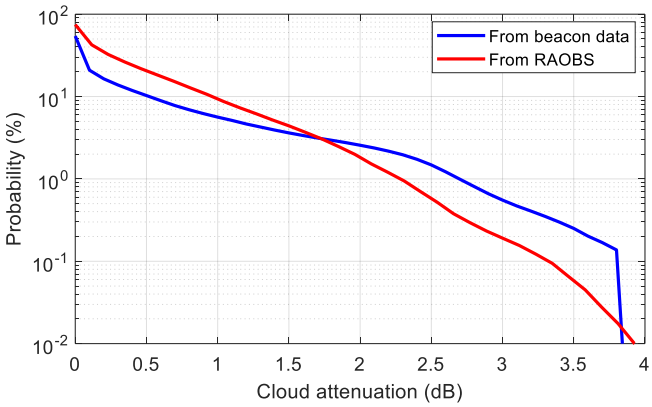

Fig. 3. CCDFs of the cloud attenuation obtained from RAOBS data (20 full years) and from the beacon data (one full year) by using equation (5) at Q band.

As is clear from the discussion above, the proposed procedure to isolate rain attenuation from the received power is more complex (but also more accurate) than the customary approach (it requires ancillary instruments, such as a MWR, and data, such as vertical atmospheric profiles) and it needs to be tailored to the available beacon data (e.g. the link frequency). Nevertheless, besides being key to properly derive the rain attenuation used in Section IV as the reference to assess the accuracy of E-SST, the proposed procedure represents a novel approach to separating the different sources of tropospheric attenuation starting from beacon data; indeed, this task becomes more and more critical as the frequency raises due to the increasingly higher contribution of clouds.

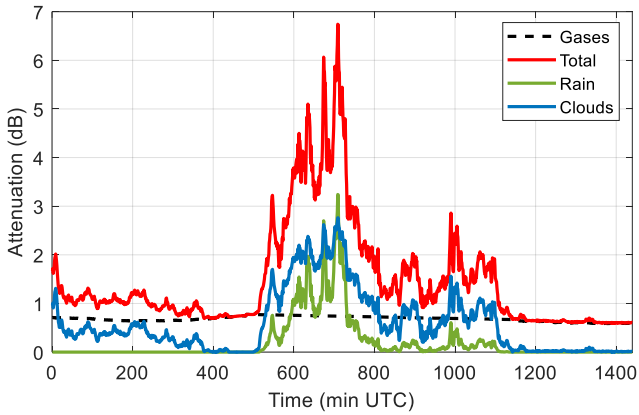

Fig. 4. Separation of the attenuation contributions due to gases, clouds and rain for a sample day (4th of February 2017) at Q band.

Fig. 5 and Fig. 6 compare the rain attenuation CCDF obtained using the proposed approach (blue line) and the excess attenuation CCDF (i.e. including the effects of precipitation and, partially, of clouds) derived using the well-established customary procedure applied in [16] (red line), at Ka and Q band, respectively. The plots confirm a relevant contribution of clouds to the excess attenuation (red line), which determines a marked discrepancy between the two curves, with a difference reaching almost 3.5 dB at Q band. This is because the proposed method to isolate rain attenuation relies on considering the cloud attenuation variability during the rain event. The rain attenuation values obtained by employing such an approach are used as the reference rain attenuation data in the remainder of this document.

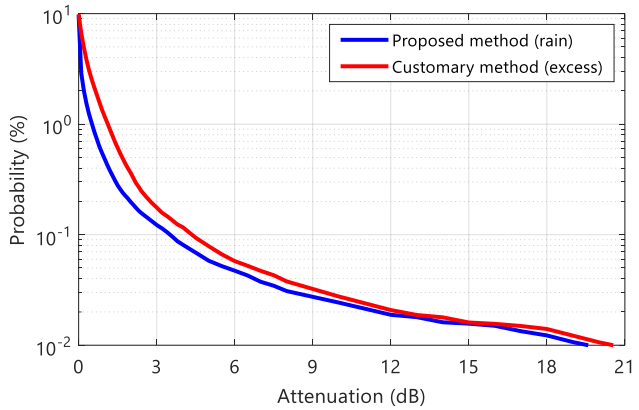

Fig. 5. CCDF of the rain attenuation obtained using the rain isolation approach proposed in this work (blue curve) and CCDF of the excess attenuation derived using the well-established customary procedure applied in [16]; Ka-band data, whole year statistics.

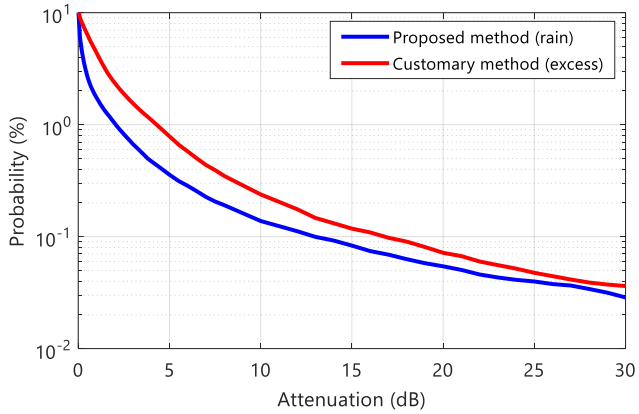

Fig. 6. CCDF of the rain attenuation obtained using the rain isolation approach proposed in this work (blue curve) and CCDF of the excess attenuation derived using the well-established customary procedure applied in [16]; Q-band data, whole year statistics.

III. The Enhanced Synthetic Storm Technique (E-SST)

Firstly introduced in [11], the Synthetic Storm Technique (SST) is a methodology to synthesize rain attenuation time series (on terrestrial links) from local rain rate observations, which relies on the frozen storm hypothesis put forth in [23]. The same concept was successfully extended to Earth-space links by Matricciani in [12] by modeling the vertical structure of precipitation with two layers (see the top side of Fig. 7): the first one (layer *A*, extending from the ground up to h_A) accounts for the attenuation induced by rain (whose intensity is R_A), while the second one (layer *B*, extending from h_A to $h_B = h_A + 0.4$ km) takes into account the impact of the melting layer, which is associated to the effective rain rate $R_B = 3.134\, R_A$. By virtue of the frozen storm hypothesis and by assuming a constant precipitation translation speed v [23], the time t can be easily turned into the distance $d = v\,t$. Thus, making reference to Fig. 7, the rain attenuation A at a given instant t_0 can be numerically calculated as:

$$A(t_0) = \frac{1}{\cos\theta}\left[\int_{d_0}^{d_0+S_A} k_A R(l)^{\alpha_A}\, dl + \int_{d_0+S_A}^{d_0+S_A+S_B} k_B 3.134^{\alpha_B} R(l)^{\alpha_B}\, dl\right] \quad (8)$$

In (8), θ is the link elevation angle, k and α are the power-law coefficients turning the rain rate into specific attenuation, which might differ for layers *A* and *B*, e.g. because of the different hydrometeor temperature and size. Finally R is the rain rate along the link, whose values are extracted from the rain intensity time series (after the conversion from time to space, $d = v\,t$) according to the geometry depicted in Fig. 7 (bottom side). The figure also clarifies how the same calculation is performed for different points in time (see t_0 and t_n).

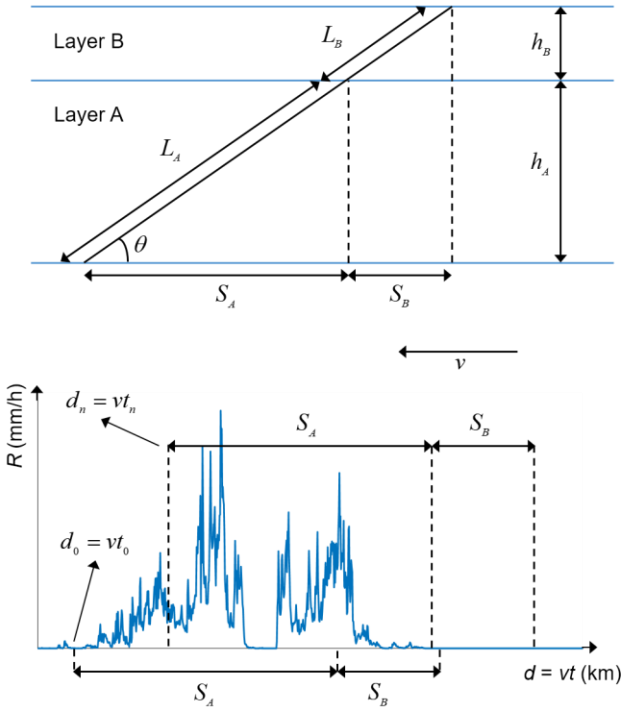

Fig. 7. Reference outline for the application of the SST: geometry of the link and of the vertical development of precipitation (top side) and identification of the rain rate values for the calculation of A_R (bottom side).

The SST has been widely used and tested, and represents a valuable tool to obtain rain attenuation time series from rain rate observations. However, the model presents a main shortcoming, which this contribution aims at overcoming. In fact, a limitation in the accuracy of the SST lies in layer *B*, which is intended to model the contribution to attenuation due to the melting layer [12]: as a matter of fact, a well-defined melting layer appears only in association to stratiform events, as the strong updrafts and downdrafts occurring during convective events create a mixture of ice, liquid water and melting particles. This point has been addressed in [24] by proposing an algorithm to discriminate between convective and stratiform events (based on whether the peak rain rate during the event exceeds 10 mm/h or not, respectively), which, in turn, allows not only including the effects of the melting layer only during the former type of events, but also employing different stratiform and convective rain heights [7].

The SST prediction accuracy can be further improved by using as input, when available, "instantaneous" values of the rain height h_0 and of the wind speed v. The following list summarizes the key features introduced into the E-SST:

1. Starting from the rain rate time series, every event is classified as convective (stratiform) if its peak rain intensity exceeds (does not exceed) 10 mm/h [24]. Events are separated by dry periods lasting at least 1 hour.
2. Differently from the SST, the melting layer attenuation is taken into account only during stratiform events and in an equivalent way; in fact, a single layer is considered: the specific rain attenuation is calculated using the k and α coefficients (see (8)) from Recommendation ITU-R P.838-3 [25] and the equivalent rain height is calculated by adding 0.36 km to h_0, as suggested in

Recommendation ITU-R P.839-4 [26]. This choice is aimed at both simplifying and updating the model by relying on the most recent coefficients recommended by ITU-R to estimate the specific attenuation due to rain.
As a result, the equivalent rain height for stratiform events is:

$$H_S = h_0 + 0.36 \quad \text{(km)} \tag{9}$$

while the equivalent rain height for convective events is:

$$H_C = h_0 \quad \text{(km)} \tag{10}$$

Both in (9) and (10), h_0 is the 0 °C isotherm height derived from ERA5 vertical profiles of temperature. For each sample in the rain event time series, h_0 is obtained as the linear interpolation between the two closest ERA5 profiles.

3. Similarly to point 3, the precipitation translation velocity v is derived from ERA5 vertical profiles, specifically by selecting the wind speed associated to the 700-mbar isobar height [15].

IV. Results and Discussion

This Section deals with the validation of the E-SST, whose results are compared with those obtained from the SST and against the reference experimental data collected in Milan in the frame of the Alphasat Aldo Paraboni propagation experiment. More specifically, first the E-SST is applied for the direct prediction of rain attenuation time series starting from rain rate data. Afterwards, the model is embedded into a more accurate frequency scaling technique. To the aim of testing the accuracy of the E-SST, we have used a full year of propagation data (2017) collected by the NASA experimental equipment installed at Politecnico di Milano (see Section II.A).

A. Rain Attenuation Prediction: Direct Application of the E-SST

Similarly to what is proposed in [12], the most straightforward application of the E-SST consists in the prediction of rain attenuation time series starting from the 1-minute sampled rain rate data using (8) and the rain heights in (9) and (10).

The top side of Fig. 8 shows the results obtained for a stratiform event (peak rain rate R < 10 mm/h) occurred on the 3rd of February 2017; the blue line represents the rain attenuation derived from the beacon measurement at 39.4 GHz, while the other curves indicate the predictions delivered by the SST (red dashed line) and the E-SST (dash-dotted green line). The bottom side of the figure reports the concurrent rain rate measured by the disdrometer.

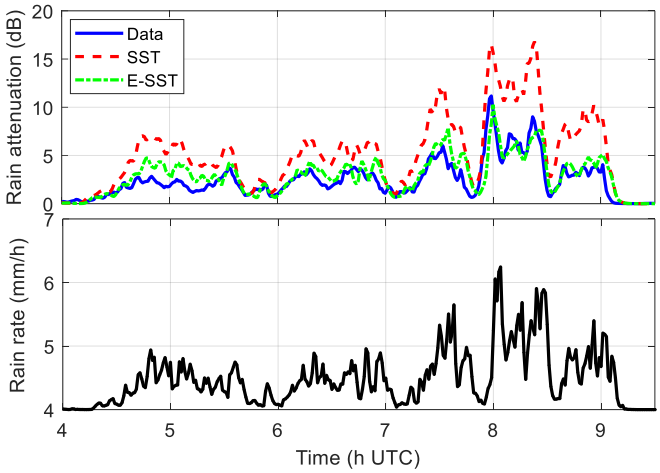

Fig. 8. Direct application of the SST and the E-SST to a stratiform rain event on the 3rd of February 2017 (peak rain rate R < 10 mm/h), at Q band.

Results indicate a higher prediction accuracy of E-SST compared to SST, which mainly results from using more precise input information. In fact, as input to the SST we have used the yearly mean value of the wind speed, $\bar{v} = 7.2$ m/s, and the yearly mean value of the 0 °C isotherm height, $\bar{h}_A = \bar{h}_0 = 3.061$ km (i.e. $\bar{h}_B = 3.461$ km), both derived from the ERA5 profiles of the whole of 2017; on the other hand, as input to E-SST, we have used the daily ERA5 values associated to the profiles ranging from 4 to 9 UTC, with v and h_0 in the 8.56-9.54 m/s range, and in the 1.783-1.845 km interval, respectively.

Another sample rain event is shown in Fig. 9, which depicts the outcomes of the application of the SST and the E-SST for a shorter but more intense convective event occurred on the 5th of May 2017 (Ka-band data). As is clear from Fig. 9, the E-SST provides significantly more accurate results than the SST: the large discrepancy between the two models is due both to the difference in the input rain height and storm velocity (in this case, during the event, h_0 ranges between 2.702 km and 2.841 km, while v varies in the 1.04-2.52 m/s range), but also to the inclusion of the melting layer effect in the SST, which is very unlikely during convective events. It is also worth noticing that, in this case, the predicted attenuation peaks appear a bit "delayed" with respect to those shown in the attenuation data likely due to the simplifying assumptions used in both models: for instance, the frozen storm hypothesis [23] (which might be more questionable for very turbulent convective events) and the fact that the rain event is inherently assumed to reach the receiver along the direction of the link.

This article has been accepted for publication in a future issue of this journal, but has not been fully edited. Content may change prior to final publication. Citation information: DOI 10.1109/TAP.2020.2981682, IEEE Transactions on Antennas and Propagation

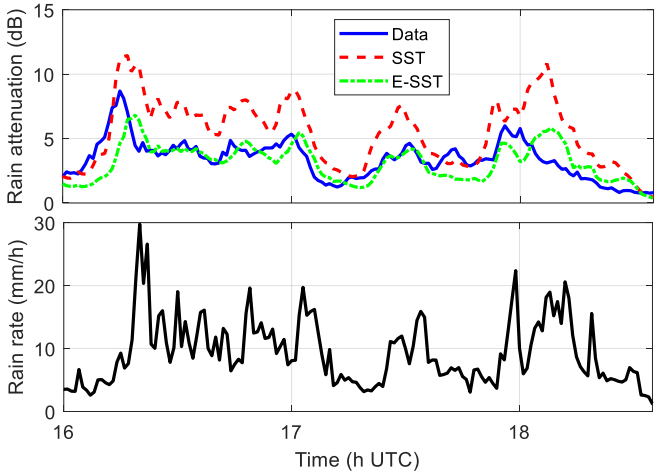

Fig. 9. Direct application of the SST and the E-SST: convective rain event on the 5th of May 2017 (peak rain rate R > 10 mm/h), Ka band data.

A more comprehensive picture of the models' prediction accuracy is given in Fig. 10 and Fig. 11, which show the complementary cumulative distribution functions (CCDFs) of rain attenuation including all events in 2017 (Ka band and Q band, respectively). The models' performance is quantified by using the following ITU-R-defined error figure [27]:

$$\varepsilon(P)=\begin{cases}100\cdot\left(\dfrac{A_R(P)}{10}\right)^{0.2}\ln\left(\dfrac{A_P(P)}{A_R(P)}\right) & A_R(P)<10\text{ dB}\\ 100\cdot\ln\left(\dfrac{A_P(P)}{A_R(P)}\right) & A_R(P)\geq 10\text{ dB}\end{cases} \quad (11)$$

In (11), $A_R(P)$ and $A_P(P)$ represent rain attenuation, both correspondent to probability level P, extracted respectively from the reference (measured data) and the estimated (model) CCDFs. Table II lists the average (E) and root mean square (RMS) values of $\varepsilon(P)$ for both models: the results confirm the marked increase in accuracy of the E-SST.

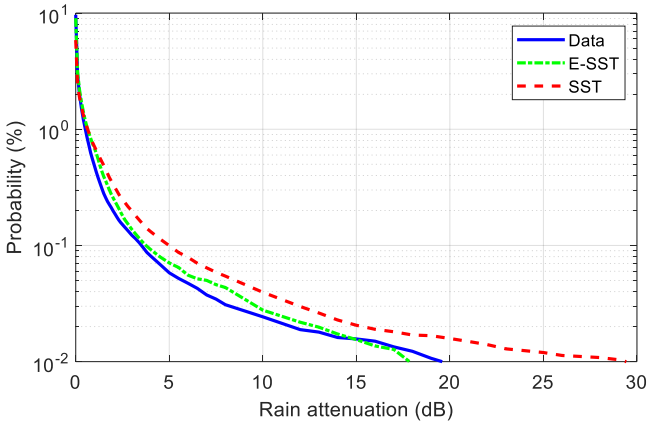

Fig. 10. Direct application of the SST and the E-SST at Ka band, whole year statistics.

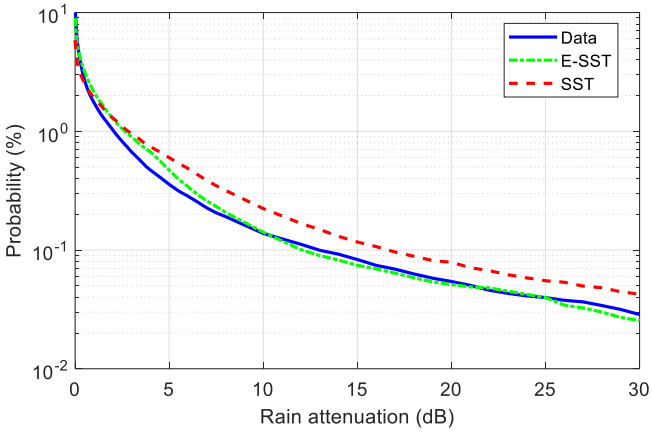

Fig. 11. Direct application of the SST and the E-SST at Q band, whole year statistics.

TABLE II. OVERALL PREDICTION ACCURACY OF THE SST AND THE E-SST (DIRECT APPLICATION): RAIN ATTENUATION CCDFS (2017), BOTH BANDS.

	E (%)		RMS (%)	
	Ka band	Q band	Ka band	Q band
SST	21.95	20.45	24.78	22.66
E-SST	4.65	2.85	8.14	5.2

B. Rain Attenuation Prediction: Frequency Scaling Based on the E-SST

When measurements of rain attenuation A along a link at frequency f_{DOWN} are available in a site, frequency scaling represents a simple yet accurate approach to predict A along the same link, but at a different frequency f_{UP}. This is achieved by means of the frequency scaling ratio R_{FS}:

$$A(f_{UP})=R_{FS}\,A(f_{DOWN}) \quad (12)$$

The accuracy of frequency scaling techniques is generally higher than the one of prediction models, as rain attenuation measurements embed key information on the rain event (e.g. spatial distribution of the rain rate, both horizontally and vertically). Moreover, when the dynamics of rain attenuation are of interest, e.g. for the investigation of fade slope and fade duration (both of which are important, for example, to properly design site diversity techniques) or for the real-time scenarios involving the application of up-link power control, frequency scaling will provide more realistic time series of the predicted rain attenuation than the application of any prediction model.

Empirical frequency scaling models exist in the literature. They are typically valid on a statistical basis and are of limited accuracy as they define a fixed value for R_{FS}, dependent only on f_{DOWN} and f_{UP}. In fact, on the contrary, R_{FS} usually changes significantly from event to event (even more, within the same event). This aspect can be duly taken into account by resorting to DSD data, on which the specific attenuation due to rain γ_{DSD} depends on [14]:

$$\gamma_{DSD}(f)=4.343\cdot 10^3\frac{\lambda^2}{\pi}\sum_{i=1}^{N}\mathrm{Re}\left[S_0(D_i,f)\right]N(D_i)\Delta D_i \quad (13)$$

In (13), N = 22 is the number of diameter classes measured

by the disdrometer, while the forward scattering coefficient S_0 is calculated using the T-matrix approach [28], assuming the axial ratio defined by Beard and Chuang in [29]. As a result, the frequency scaling ratio R_{FS} is defined as:

$$R_{FS}^{DSD}(t_0) = \frac{\gamma_{DSD}(t_0, f_{UP})}{\gamma_{DSD}(t_0, f_{DOWN})} \quad (14)$$

Though this approach offers a very good frequency scaling accuracy [30], the availability of DSD data is usually quite rare. As an alternative, the frequency scaling ratio R_{FS} can be defined by taking advantage of the E-SST:

$$R_{FS}^{E-SST}(t_0) = \frac{A(t_0, f_{UP})}{A(t_0, f_{DOWN})} \quad (15)$$

where both $A(t_0, f_{UP})$ and $A(t_0, f_{DOWN})$ are calculated according to the mathematical framework of the E-SST.

Fig. 12 and Fig. 13 show the variability of the frequency scaling ratio for the two events reported in Fig. 8 and Fig. 9, respectively, both as derived from the E-SST and from DSD data. Moreover, as a term of comparison, also included in Fig. 12 and Fig. 13 is the frequency scaling ratio defined by the statistical model included in Recommendation ITU-R P.618-13 [31] (blue solid line), for which R_{FS} marginally depends also on $A(f_{DOWN})$, besides on f_{DOWN} and f_{UP}.

As is clear from Fig. 12 and Fig. 13, R_{FS}^{DSD} is highly variable even within the same event: while R_{FS}^{E-SST} tends to follow the same trend as R_{FS}^{DSD}, the frequency scaling ratio defined by the ITU-R is much more stable and thus unable to provide an accurate frequency scaling.

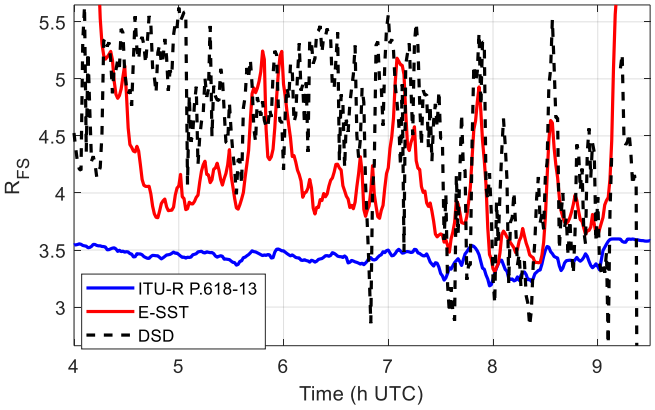

Fig. 12. Frequency scaling ratio R_{FS} for the same stratiform event in Fig. 8 as calculated using the E-SST model and DSD data, as well as derived from the model included in Recommendation ITU-R P.618-13.

Fig. 14 and Fig. 15 show the time series obtained by scaling the attenuation measured at 19.7 GHz to 39.4 GHz, using the E-SST and DSD data. As expected, results indicate that both methods provide a further prediction improvement achieved by using the frequency scaling approach, if compared to the direct application of the E-SST. More importantly, results show that an accurate frequency scaling can be obtained even by just using the E-SST, i.e. without the need of DSD data, which, as already mentioned, are seldom available and are used in this work as a the reference upper limit of the prediction accuracy using frequency scaling techniques.

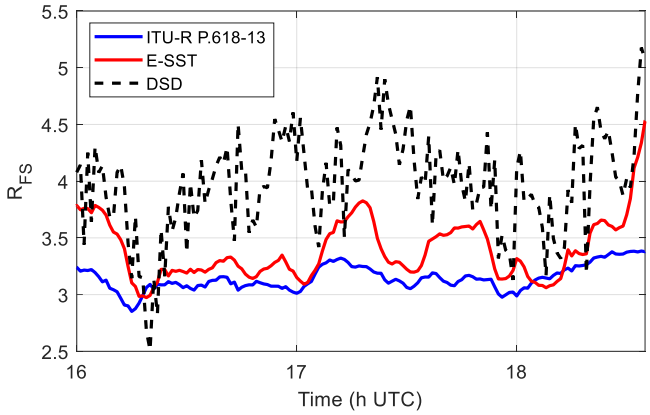

Fig. 13. Frequency scaling ratio R_{FS} for the same convective event in Fig. 9 as calculated using the E-SST model and DSD data, as well as derived from the model included in Recommendation ITU-R P.618-13.

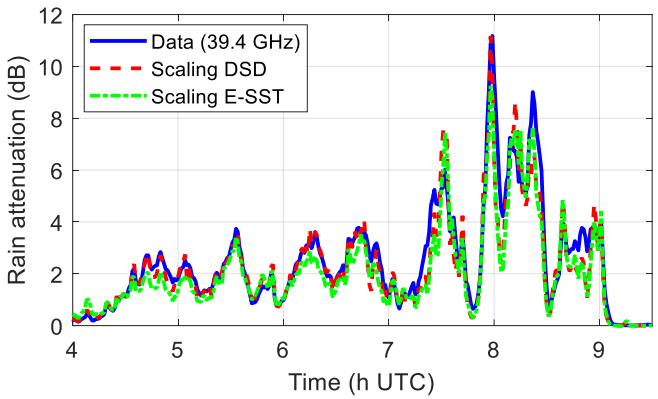

Fig. 14. Scaling of the attenuation measured at 19.7 GHz to 39.4 GHz for the stratiform rain event on the 3rd of February 2017 (peak rain rate R < 10 mm/h) in Fig. 8.

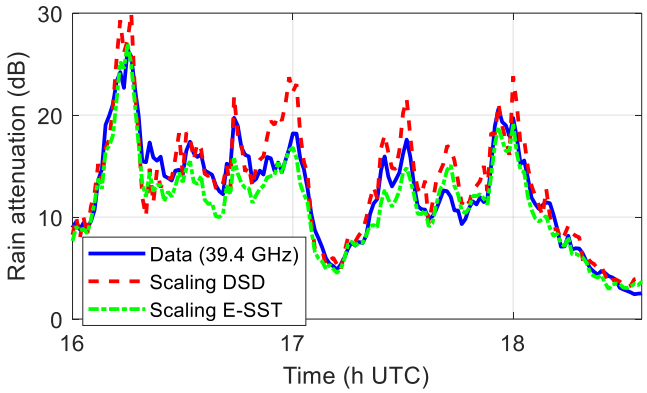

Fig. 15. Scaling of the attenuation measured at 19.7 GHz to 39.4 GHz for the convective rain event on the 5th of May 2017 (peak rain rate R > 10 mm/h) in Fig. 9.

In line with the results reported in Fig. 14 and Fig. 15, as expected, the frequency scaling approach offers an overall enhancement in the prediction of the CCDF of A(39.4 GHz): the bias improves and the RMS of the error figure in (11), reported in Table III, lowers to 4.8% and 3.9%, using the

E-SST and DSD data, respectively (values to be compared with the results listed in Table II).

TABLE III. OVERALL PREDICTION ACCURACY USING THE FREQUENCY SCALING APPROACH: RAIN ATTENUATION CCDFS (2017), Q BAND.

	E (%)	RMS (%)
	Q band	Q band
E-SST (frequency scaling)	-3.5	4.83
DSD (frequency scaling)	1.5	3.89

Even more marked is the decrease in the prediction error on the time series of the attenuation, which is quantified by using E and RMS of the absolute error figure in (16).

$$\phi(t) = A_p(t) - A_R(t) \tag{16}$$

Results, reported in Table IV, confirm the improvement associated to the frequency scaling approach using the E-SST, if compared to the direct application of the model. Included in the table is also the performance of the reference frequency scaling technique relying on DSD data.

TABLE IV. OVERALL PREDICTION ACCURACY OF THE E-SST (BOTH DIRECT APPLICATION AND FREQUENCY SCALING APPROACH) ON RAIN ATTENUATION TIME SERIES (2017), Q BAND. INCLUDED IS ALSO THE PERFORMANCE OF REFERENCE FREQUENCY SCALING USING DSD DATA.

	E (dB)	RMS (dB)
E-SST (direct application)	-0.11	2.99
E-SST (frequency scaling)	-0.05	1.77
DSD (frequency scaling)	-0.05	1.72

V. CONCLUSIONS

This contribution described the Enhanced Synthetic Storm Technique (E-SST), a new model introducing improvements to the original Synthetic Storm Technique (SST). The specific novel key features of the E-SST are: 1) it receives as input detailed information on the rain height and on the storm velocity, which, in this work, are extracted from ECMWF NWP products every hour (ERA5 database); 2) it discriminates between stratiform and convective events; 3) it makes use of different rain heights depending on the type of event.

The accuracy of E-SST was tested against a full year (2017) of propagation data collected by the NASA equipment installed at Politecnico di Milano in the frame of the Alphasat Aldo Paraboni propagation experiment. To this aim, a novel approach to isolate rain attenuation from the received beacon power was devised and presented. The accuracy in reproducing the CCDF of *A* (both at 19.7 and 39.4 GHz) was first evaluated by directly applying the E-SST; compared to the SST, the RMS of the (ITU-R defined) error figure reduces from 24.8% (SST) to 8.1% (E-SST) at Ka band and from 22.7% (SST) to 5.2% (E-SST) at Q band. A further improvement in the prediction performance was achieved by embedding the E-SST into a more accurate frequency scaling technique, i.e. by using as an additional input to the model also *A* measured at 19.7 GHz, with the RMS of the error on first-order statistics reaching 4.83% (Q band). The advantage of using such a frequency scaling approach is even more visible when the time series of *A* are considered: results show that the frequency scaling accuracy achieved by using the E-SST is approximately comparable to the one obtained by relying on DSD data, which, however, are seldom available: the RMS of the absolute error at Q band is 1.8 dB and 1.7 dB using E-SST and DSD data, respectively.

Though further data are needed to corroborate the accuracy of the E-SST, the results obtained in this work are encouraging and suggest that the E-SST is a physically-based accurate and reliable tool for the prediction of rain attenuation at EHF, both on a statistical basis (direct application) and on an event basis (frequency scaling approach).

ACKNOWLEDGMENT

The authors would like to acknowledge: the Agenzia Spaziale Italiana (ASI), in particular Giuseppe Codispoti, for supporting the Alphasat Aldo Paraboni propagation experiment; NASA for making available the experimental data within the collaboration with Politecnico di Milano on the Alphasat Aldo Paraboni propagation experiment; ECMWF for providing vertical atmospheric profiles.

This effort was supported in part by the Air Force Office of Scientific Research, Air Force Material Command, USAF, under grant number FA9550-17-1-0335. The U.S Government is authorized to reproduce and distribute reprints for Governmental purpose notwithstanding any copyright notation thereon.

REFERENCES

[1] C. Riva, C. Capsoni, L. Luini, M. Luccini, R. Nebuloni, A. Martellucci, "The Challenge of Using the W Band in Satellite Communication," *Int. J. Satell. Commun. Network.* 2014; 32:187–200.

[2] R. K. Crane, "Electromagnetic Wave Propagation Through Rain," New York, Wiley, 1996.

[3] T. Rossi, F. Maggio, M. De Sanctis, M. Ruggieri, S. Falzini, M. Tosti, "System analysis of smart gateways techniques applied to Q/V-band high throughput satellites," *IEEE Aerospace Conference*, pp. 1-10, 1-8 March 2014, Big Sky, Montana, USA.

[4] M. Biscarini, F. S. Marzano, M. Montopoli, K. De Sanctis, L. Iess, M. Montagna, M. Mercolino, M. Lanucara, "Optimizing Data Volume Return for Ka-Band Deep Space Links Exploiting Short-Term Radiometeorological Model Forecast," *IEEE Transactions on Antennas and Propagation*, vol. 64, issue 1, pp. 235-250, Jan. 2016.

[5] EOARD Award FA8655-12-1-2062, "Performance evaluation of Satellite Communication systems operating in the Q/V/W band".

[6] L. Luini, C. Capsoni, "A Rain Cell Model for the Simulation and Performance Evaluation of Site Diversity Schemes," *IEEE Antennas and Wireless Propagation Letters*, vol. 12, No. 1, Page(s): 1327-1330, 2013.

[7] C. Capsoni, L. Luini, A. Paraboni, A. Martellucci, "A New Prediction Model of Rain Attenuation That Separately Accounts for Stratiform and Convective Rain," *IEEE Transactions on Antennas and Propagation*, Vol 57, No. 1, Page(s): 196 – 204, January 2009.

[8] G. H. Bryant, I. Adimula, C. Riva, G. Brussaard, "Rain attenuation statistics from rain cell diameters and heights," *Int. J. Satellite Commun.*, vol. 19, no. 3, pp. 263–283, 2001.

[9] A Dissanayake, J.E. Allnutt, F. Haidara, "A prediction model that combines rain attenuation and other propagation impairments along Earth-space paths," *IEEE Transactions on Antennas and Propagation* 45 (10): 1546 – 1558, November 1997.

[10] X. Boulanger, L. Feral, L. Castanet, N. Jeannin, G. Carrie, F. Lacoste, "A Rain Attenuation Time-Series Synthesizer Based on a Dirac and

Lognormal Distribution," *IEEE Transactions on Antennas and Propagation*, vol. 61, issue 3, pp. 1396-1406, March 2013.

[11] G. Drufuca, "Rain attenuation statistics for frequencies above 10 GHz from rain gauge observations," *J. Rech. Atmos.*, 1-2, 399-411, 1974.

[12] E. Matricciani, "Physical-mathematical model of the dynamics of rain attenuation based on rain rate time series and two layer vertical structure of precipitation," *Radio Science*, Vol. 31, No. 2, March-April 1996, pages 281-295.

[13] T. Rossi, M. De Sanctis, M. Ruggieri, C. Riva, L. Luini, G. Codispoti, E. Russo, G. Parca, "Satellite Communication and Propagation Experiments Through the Alphasat Q/V Band Aldo Paraboni Technology Demonstration Payload," *IEEE Aerospace and Electronic Systems Magazine*, Vol. 31, No. 3, Page(s): 18 – 27, March 2016.

[14] L. Luini, G. Roveda, M. Zaffaroni, M. Costa, C. Riva, "EM Wave Propagation Experiment at E Band and D Band for 5G Wireless Systems: Preliminary Results," *EuCAP 2018*, 9-13 April 2018, pp. 1-5, London, UK.

[15] L. Luini, N. Jeannin, C. Capsoni, A. Paraboni, C. Riva, L. Castanet, J. Lemorton, "Weather radar data for site diversity predictions and evaluation of the impact of rain field advection," *Int. J. Satell. Commun. Network.* 2011; 29:79–96.

[16] X. Boulanger, B. Benammar, L. Castanet, "Propagation Experiment at Ka-Band in French Guiana: First Year of Measurements," *IEEE Antennas and Wireless Propagation Letters*, Vol. 18, No. 2, pp. 241-244, 2019.

[17] X. Boulanger, B. Gabard, L. Casadebaig, L. Castanet, "Four Years of Total Attenuation Statistics of Earth-Space Propagation Experiments at Ka-Band in Toulouse," *IEEE Transactions on Antennas and Propagation*, vol. 63, no. 5, pp. 2203-2214, May 2015.

[18] L. Luini, C. Riva, R. Nebuloni, M. Mauri, J. Nessel, A. Fanti, "Calibration and Use of Microwave Radiometers in Multiple-site EM Wave Propagation Experiments," *EuCAP 2018*, 9-13 April 2018, pp. 1-5, London, UK.

[19] Recommendation ITU-R P.840-7, "Attenuation due to clouds and fog," December 2017.

[20] L. Luini, C. Riva, C. Capsoni, A. Martellucci, "Attenuation in non rainy conditions at millimeter wavelengths: assessment of a procedure," *IEEE Transactions on Geoscience and Remote Sensing*, pp. 2150-2157, Vol. 45, Issue 7, July 2007.

[21] E. Salonen, W. Uppala, "New prediction method of cloud attenuation," *Elect. Lett.*, vol. 27, no. 12, pp. 1106–1108, 1991.

[22] H. J. Liebe, G. A. Hufford, M. G. Cotton, "Propagation modelling of moist air and suspended water/ice particles at frequencies below 1000 GHz," *AGARD 52nd Specialists' Meeting of The EM Wave Propagation Panel*, Palma De Maiorca, Spain, 1993.

[23] G. I. Taylor, "The spectrum of turbulence," *Proc. R. Soc. London A*, 164, 476-490, 1938.

[24] C. Capsoni, L. Luini, A. Paraboni, C. Riva, "Stratiform and convective rain discrimination deduced from local $P(R)$," *IEEE Transactions on Antennas and Propagation*, vol. 54, issue 11, pp. 3566-3569, Nov. 2006.

[25] Recommendation ITU-R P.838-3, "Specific attenuation model for rain for use in prediction methods," Geneva, 2005.

[26] Recommendation ITU-R P.839-4, "Rain height model for prediction methods," Geneva, 2013.

[27] Recommendation ITU-R P.311-14, "Acquisition, presentation and analysis of data in studies of radiowave propagation," Geneva, 2013.

[28] M. Mishchenko, L. Travis, A. Lacis, "Scattering, Absorption, and Emission of Light by Small Particles," *Cambridge University*, 2002.

[29] K. Beard, C. Chuang, "A New Model for the Equilibrium Shape of Raindrops," *Journal of the Atmospheric Sciences*, Vol. 44, No. 11, pp. 1509 – 1524, 1987.

[30] J. Nessel, M. Zemba, L. Luini, C. Riva, "Comparison of Instantaneous Frequency Scaling from Rain Attenuation and Optical Disdrometer Measurements at K/Q bands," *21st Ka and Broadband Communications, Navigation and Earth Observation Conference*, Bologna (Italy), pp. 1-10, 12-14 October, 2015.

[31] Recommendation ITU-R P.618-13, "Propagation data and prediction methods required for the design of Earth-space telecommunication systems," Geneva, 2017.